ECS Transactions, 35 (1) 823-830 (2011)
10.1149/1.3570063 ©The Electrochemical Society

First Principles Modeling of Oxygen Mobility in Perovskite SOFC Cathode and Oxygen Permeation Membrane Materials

E. A. Kotomin[1,2], R. Merkle[1], Yu. A. Mastrikov[2,3], M. M. Kuklja[3], J. Maier[1]

[1]Max Planck Institute for Solid State Research, Heisenbergstr.1, Stuttgart, Germany
[2]Institute for Solid State Physics, University of Latvia, Kengaraga str. 8, Riga, Latvia
[3] Materials Science and Eng. Dept., University of Maryland, College Park, USA

Based on first principles DFT calculations, we analyze activation energies of oxygen vacancy migration in several complex ABO_3-type perovskite candidate materials for SOFC cathodes and permeation membranes ($La(Co,Fe)O_{3-\delta}$ (LCF) and $(Ba,Sr)(Co,Fe)O_{3-\delta}$ (BSCF)). The atomic relaxation, charge redistribution and energies of the transition states of oxygen migration are compared to understand the microscopic origin of the exceptionally low migration barrier (high oxygen mobility) in BSCF. It is shown that the B-O distance is considerably shortened in the transition state for BSCF due to covalency of this chemical bond, which could be a reason for the significant reduction of the oxygen migration energy in this material. Additionally, the Goldschmidt tolerance factor based on Shannon ionic radii is revisited.

Introduction

Owing to the high mobility of oxygen vacancies, mixed conducting $ABO_{3-\delta}$ perovskites (A=Ln, Ba, Sr and B=Mn, Fe, Co) are applied for oxygen permeation membranes as well as for cathodes in solid oxide fuel cells. $SrCo_{0.8}Fe_{0.2}O_{3-\delta}$ exhibits a high oxygen permeation rate in its cubic high-temperature phase (1). To suppress the phase-transformation into a vacancy-ordered low-temperature phase (Brownmillerite structure) with the low vacancy mobility, a B-site substitution was attempted (see e.g. (2,3,4)). An A-site substitution finally resulted in the highly oxygen-permeable perovskite $Ba_{0.5}Sr_{0.5}Co_{0.8}Fe_{0.2}O_{3-\delta}$ (BSCF5582), which remains cubic even at room temperature (5). Interestingly, BSCF5582 proved to have also a high catalytic activity for the oxygen exchange surface reaction (6). The correlation of the effective rate constant of the surface reaction with both an increase of the oxygen vacancy concentration and mobility in BSCF perovskites with various Ba/Sr and Co/Fe ratios indicated that the vacancy migration is decisive also for the surface chemistry (7). The vacancy migration barrier of $\approx$ 0.5 eV in BSCF5582 (6,8) is found to be significantly lower than the typical value of 0.8-0.9 eV for $(La,Sr)(Mn,Fe,Co)O_{3-\delta}$ perovskites (9,10). While this is in good agreement with the first DFT studies on oxygen vacancy migration in BSCF (11,12) and BCF (13) perovskites, we try here to achieve a deeper understanding of the implications for fast oxygen diffusion.

Computational Details

In calculations, density functional theory (DFT) was used, as implemented in the computer code VASP 4.6 (14) within the projector-augmented wave approach (PAW)

and the exchange-correlation PBE (GGA-type) functional (15). The kinetic energy cut-off for the plane wave basis set was 520 eV. For O, we used soft PAW pseudopotentials, which give a very good binding energy and a reasonable bond length for a free O_2 molecule (5.24 eV and 1.29 Å, cf. the experimental values of 5.12 eV and 1.21 Å, respectively). The 8×8×8 k-point mesh was created by the Monkhorst-Pack scheme (16) for the ABO_3 unit cell. Ionic charges were calculated by the Bader method (17). Oxygen vacancies were simulated using the supercells through expanding the ABO_3 primitive unit cell by 2×2×2 (40 atoms). For more details see (11). In the DFT calculations, the cation composition $Ba_{0.5}Sr_{0.5}Co_{0.75}Fe_{0.25}O_{3-\delta}$ is used as good approximation to the experimentally most studied BSCF5582 material.

Results and Discussion

The Shannon ion radii (18) are derived from crystallographic atomic distances, and, while they work well for predicting cation-anion distances, the underlying individual ionic radii might be less reliable. Nevertheless, these individual ionic radii are also used frequently, e.g. when considering structural aspects, such as the stability of cubic perovskites based on the Goldschmidt tolerance factor. To a certain degree, they are also useful for the discussion of ionic mobility in perovskites (19). According to the Shannon radii (for the appropriate coordination numbers), in the BSCF perovskites, the A site cations Ba^{2+} and Sr^{2+} have almost the same sizes (1.61 Å and 1.45 Å) as the oxygen ion (1.36 Å), while B site cobalt and iron ions are much smaller (approx. 0.55-0.65 Å depending on spin and the oxidation state).

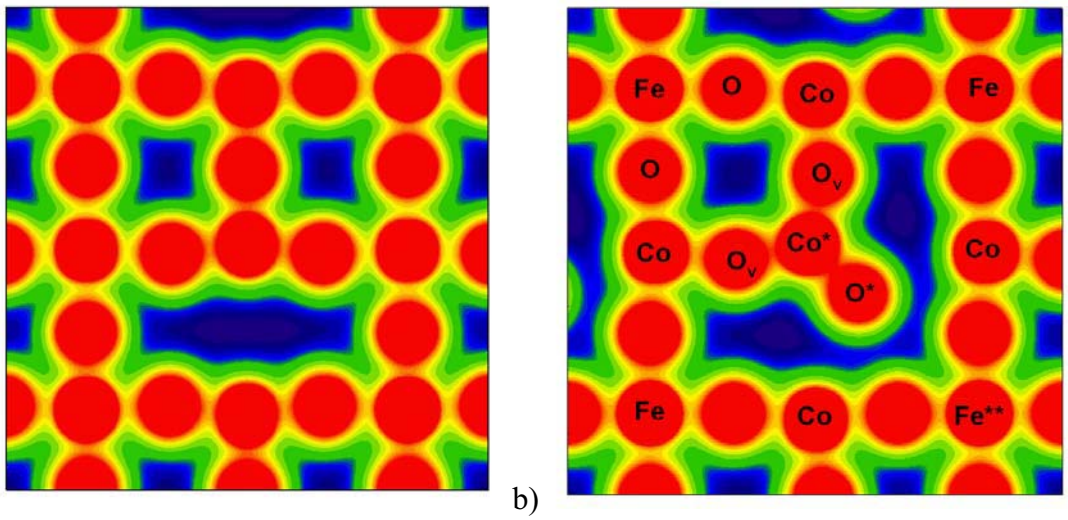

Figure 1. The electron density maps of BSCF5582 in the (001) plane from DFT calculations. a) initial (equilibrium) state, b) transition state of oxygen migration (note the logarithmic scaling, ranging from 0.01 - 1 e/Å^3; values higher than one appear in red).

However, the electronic density maps of BSCF and LCF perovskites shown in Figs. 1 and 2 indicate that the traditional Shannon ionic radii have to be taken with caution. Clearly, Ba^{2+} and Sr^{2+} are the biggest ions, but oxygen and Co/Fe ions have almost the same size. While according to the Shannon radii, La^{3+} (1.36 Å for coordination number 12) should be comparable to Sr^{2+}, it appears to be rather comparable to Ba^{2+} from Fig.1. The calculated lattice constants of $LaCoO_3$ (LC) and $LaFeO_3$ (LF) are slightly smaller

than those of (Ba,Sr)CoO_3 (BSC) and (Ba,Sr)FeO_3 (BSF). The trend is in general agreement with experimental lattice constants, although the difference in the oxygen deficiency in (La,Sr)(Co,Fe)$O_{3-\delta}$ and BSCF complicates their comparison. This also means that more space exists between the A cations and the oxygen ions than expected for a perovskite lattice with the Goldschmidt factor *t* close to 1 (for t ≈ 1, oxygen ions together with A cations are arranged in a cubic close packing). Fig. 2 illustrates that in the transition state of an oxygen migration, a significant tilting of the CoO_6 octahedron can occur, which facilitates the passing of the migrating oxygen between the larger Ba^{2+} and smaller Sr^{2+} ions (a more detailed discussion follows).

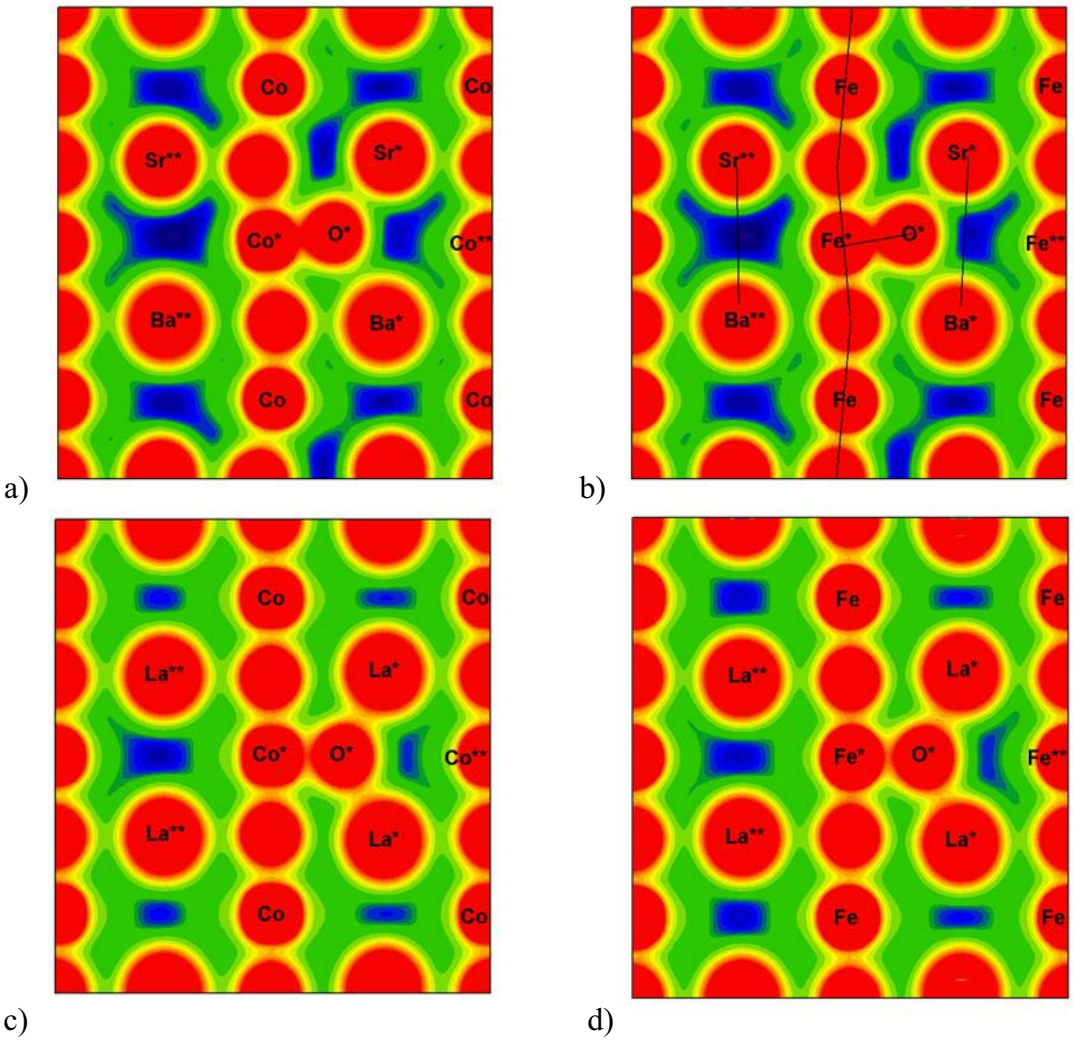

Figure 2. The electron density maps of a) BSC, b) BSF, c) LC and d) LF in the (110) plane for the transition state of O^* ion migration. The black lines in the BSF plot emphasize the structure deformations caused by O^* migration (a similar distortion pattern occurs for BSC, but is absent for LC, LF).

For a better understanding of the oxygen migration in BSCF perovskites, we compare below the migration barriers and structural aspects for several perovskites with the cubic or nearly cubic structures: BSC, BSCF5582, BSF, LC, and LF. BSCF5582 and BSF remain cubic even at low temperature, while LC and LF exhibit slight deviations from a cubic symmetry. Despite the fact that experimentally BSC has a driving force to transform into the hexagonal perovskite structure (20), its structural features and the

oxygen migration barrier in the cubic phase are very close to those of BSCF5582 so that the "cubic" approximation for BSC seems to be justified. The fact that the shape of the 2×2×2 supercell was kept cubic does not exclude local distortions and displacements within the supercell as a full relaxation was taken into account in calculations. Test calculations have shown that lifting the cubic symmetry practically does not affect results. Fig. 3 shows the supercells for BSC and LF containing one oxygen vacancy each. The two neighboring Co or Fe are slightly displaced, which also induces a slight bending of most Co/Fe-O-Co/Fe bonds and some Co/Fe-O bond length alternation (± 4%).

TABLE I. Structural and energetic parameters of O migration in BSC, BSF, LC and LF. O* indicates the migrating oxygen in the transition state; O_v, O_h and A*, B*, B** are assigned in Figs. 1, 2 (for the respective bonds of slightly different lengths, the average is given). Italic numbers give the change in the transition state relative to the ideal structure crystal. Δq(O*) is the change of O* ion charge in the transition state relative to the initial state. For BSCF5582, the geometry and barrier from an Co-O-Co initial state to a Co-O-Co final state as well as for Fe-O-Co to Fe-O-Co (Fe*-O* transition state) is given.

lattice const. migr. barrier	d(B*-O*) / Å	d(B*-O_v) / Å	d(B*-O_h) / Å	q(O*)/e_0 Δq(O*)/e_0	Δd(B*-B**) / Å	d(A*-O*) / Å
BSC 3.90 Å 0.40 eV	1.70 *-13%*	1.77 *-9%*	1.95 *±0%*	-0.97 *+0.10*	0.16 *+3%*	2.37, 2.58 aver. 2.48
BSCF5582 3.90 Å 0.42 eV Co*-O*	1.69 *-13%*	1.77 *-9%*	1.98 *+1.5%*	-0.98 *+0.09*	0.23 *+4%*	2.38, 2.59 aver. 2.49
0.46 eV Fe*-O*	1.69 *-13%*	1.76 *-10%*	1.91 *-2%*	-0.95 *+0.13*	0.13 *+2%*	2.39, 2.57 aver. 2.48
BSF 3.92 Å 0.72 eV	1.68 *-14%*	1.78 *-9%*	1.95 *±0%*	-0.96 *+0.12*	0.14 *+3%*	2.40, 2.57 aver. 2.49
LC 3.83 Å 0.76 eV	1.78 *-7%*	1.85 *-4%*	1.91 *±0%*	-1.16 *+0.02*	0.06 *+1%*	2.28
LF 3.88 Å 0.75 eV	1.84 *-5%*	1.96 *+1%*	1.91 *-1.5%*	-1.25 *±0.00*	-0.04 *-0.7%*	2.26

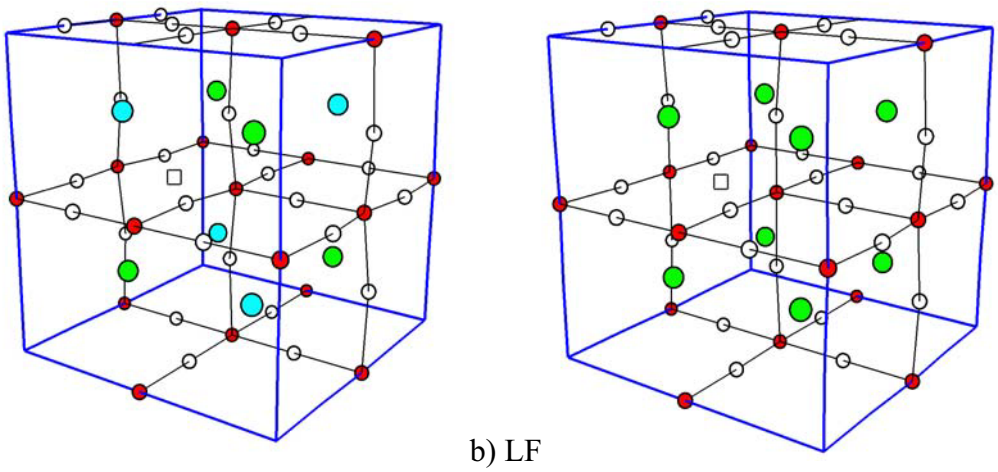

a) BSC b) LF

Figure 3. a) BSC (Ba = green, Sr = cyan, Co = red, O = white) and b) LF (La = cyan, Fe = red, O = white) 2×2×2 supercells containing one oxygen vacancy = empty square (initial state of oxygen migration). On the outer faces some atoms are omitted for clarity.

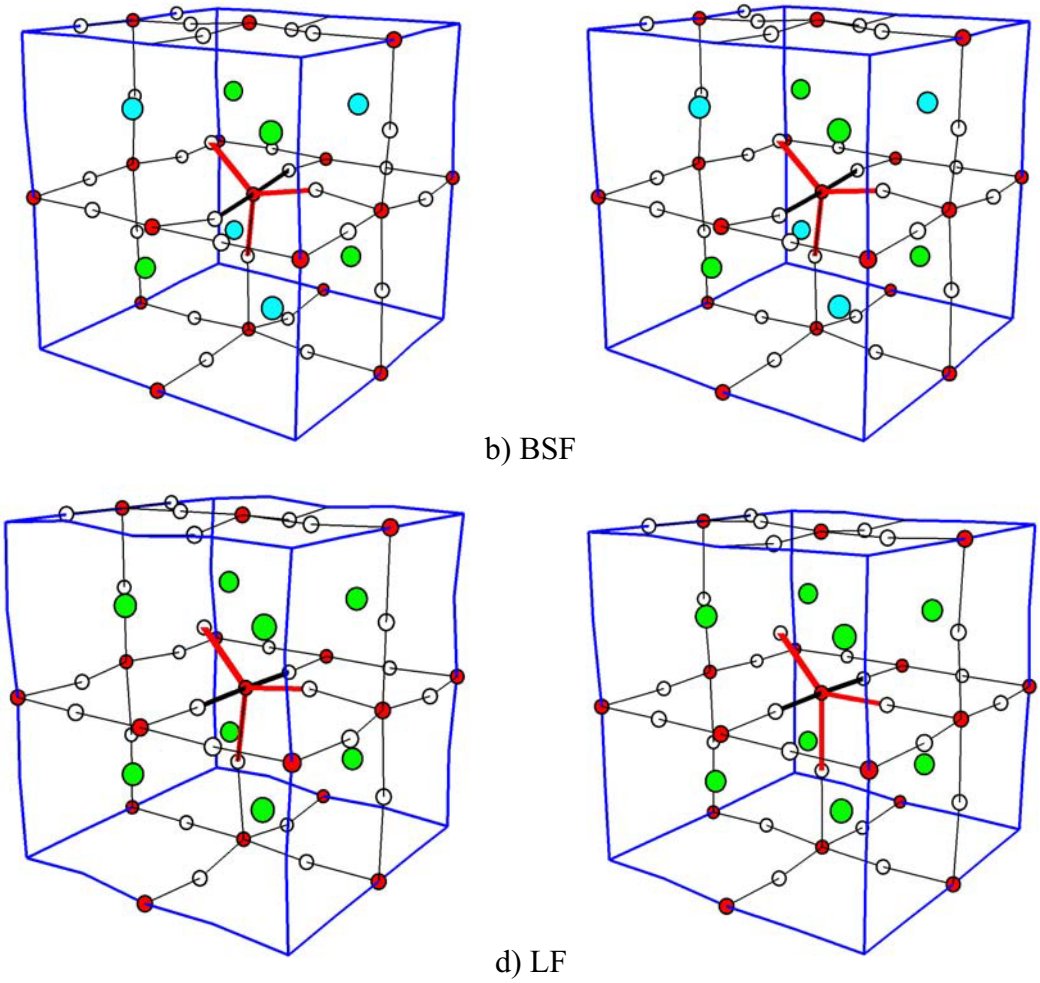

Figure 4. The transition state of oxygen migration in: a) BSC, b) BSF, c) LC and d). Red color indicates significantly shortened B*-O* and B*-O bonds. The bold black lines show the axis of the $B^*O_4O^*$ polyhedron, which is tilted in BSC, BSF but untilted in LC, LF. On the outer faces some atoms are omitted for clarity.

Table I collects important structural details together with the calculated oxygen migration barriers. The barrier height of 0.40 eV for BSC (comparable to 0.42-0.49 eV calculated for BSCF5582) (11) is in good agreement with the experimental value of 0.5 eV (8). Its increase to 0.72 eV in BSF also corresponds to the experimental trend (1.0 eV (7)), although the quantitative agreement is poorer. Finally, the calculated similar barriers for LF and LC of ≈ 0.8 eV (11) agree well with experimental data (9,10).

Fig. 4 shows a sketch of the transition states of oxygen migration in BSC and LF. It is obvious that not only the direct environment of the migrating oxygen is distorted, but the whole region around (within 6-8 Å) exhibits modified bond lengths and angles. In general, these deformations are a bit stronger for BSC and LC compared to BSF and LF. The migrating oxygen (O*) has to pass through a triangle formed by one B cation and two A cations, which is too narrow without lattice distortions. The resulting close ion contacts are best visible in the electronic density plot (Fig. 2). BSC and BSF show a tilting of the BO_4O^* polyhedron resulting from the difference in Ba^{2+} and Sr^{2+} sizes. In these two perovskites, the Sr* is also significantly displaced away from the jumping O*.

However, in LC and LF (with La^{3+} being effectively larger than Sr^{2+}) such a displacement is restricted by the proximity of the next regular oxide ion; thus only a slight elongation of the La*-La* is possible here. As a result, the La*-O* distance is shorter by ≈ 0.2 Å than the averaged A*-O* distance in BSC, BSF (last column in Table I) which is expected to increase the barrier.

The passage of O* through the A_2B triangle can be facilitated by several factors:

(i) Displacement of A cations from the jumping O* ion.

(ii) Outward displacement of a whole BO_4O^* polyhedron.

(iii) Modification of B-O* bond character (electron transfer from O* to B* decreases the effective diameter of O*. This can alternatively be interpreted as an increased covalence contribution into the chemical bonding, thus also shortening the Co*-O* bond length).

The A-O* bond character is essentially ionic and not expected to change much (even for the most polarizable A cation, Ba^{2+}, there is no sign of a visible deformation in the electron density). Table I indicates however that severe electronic as well as geometrical rearrangements occur in the transition state.

Let us discuss the possibilities (i) to (iii) in more detail for the BSCF and LCF perovskites. In all cases, the necessity to squeeze O* through the A_2B triangle is the starting point for diffusion, but the perovskites under study react differently, which finally results in quite different migration barriers.

(i) A* displacement: in BSCF, the smaller Sr* has some space to move away from O* (and even the averaged Ba*-O*, Sr*-O* distances are significantly longer than La*-O* in LCF, see the last column in Table I). Thus, one could expect a lower barrier for one or two Sr^{2+} in the A_2B triangle compared to the Ba_2(Co/Fe) case (this will be checked in further calculations). Due to the smaller lattice constant despite La^{3+} having almost the same size as Ba^{2+}, the A* cations in LCF can hardly move away from O*.

(ii) Displacement of BO_4O^* polyhedron: some strain can be released in BSCF by an outward move of the whole BO_4O^* polyhedron (see column 6 in Table I), which is much less pronounced in LCF.

(iii) Modification of the B-O* bond character: this "covalency effect" is stronger in BSCF than in LCF (see the B*-O* bond length and Δq(O*), columns 2 and 5 in Table I). The interpretation is not unambiguous; several aspects have to be discussed. One is the higher formal oxidation state of the transition metals in BSCF compared to LCF, which implies a stronger tendency for the electronic density transfer from O*. The other is the local *electrostatic* interaction of the jumping oxygen with its environment. In BSCF, O* has two Ba^{2+}/Sr^{2+} cation neighbors (effective cation charge ≈ -1.6 e_0), while in LCF, the A cation has a formal charge of 3+ (effective charge ≈ -1.95 e_0). The stronger electrostatic attraction of electrons on O* towards La^{3+} in LCF may be a reason for the smaller O*→B* electron density transfer, and could also contribute to the A*-O* bond shortening. Finally, at the moment it is not possible to decide how much the tilting

of the BO_4O^* polyhedron (observed in BSCF) is important for the "covalency effects" (the related bending of the vertical B*-O-B bonds probably weakens these bonds and - for a compensation - strengthens and shortens the equatorial B*-O* bond).

The higher O migration barriers for LCF could be understood by all the relaxation mechanisms (i) to (iii) above being less favorable than for BSCF, in combination with the smaller lattice constant. The higher barrier for BSF compared to BSC probably arises from the fact that the energy cost for the charge transfer from oxygen, corresponding to a partial reduction of the B cation, is higher for Fe compared to Co - keeping in mind the more negative oxidation enthalpy of BSF (11).

Interestingly, the ionic conductivity of BSCF5582 (calculated from D^* (8)) is by a factor of four larger than that of the best perovskite-structure electrolyte $La_{0.8}Sr_{0.2}Ga_{0.8}Mg_{0.2}O_{2.8}$ (21). This could be related to the transition state in BSCF involving not only geometrical relaxations but also a significant *electron* transfer from O* to the transition metal ions Co/Fe.

Summary

The DFT first principles calculations for 40 atom supercells containing a single oxygen vacancy yield O migration barriers ranging from 0.40 eV for $Ba_{0.5}Sr_{0.5}CoO_{2.875}$ to ≈ 0.75 eV for $LaCoO_{2.875}$ and $LaFeO_{2.875}$, in good agreement with experimental data. The analysis of the transition state energy and atomic configuration indicates it comprises a delicate combination of structural rearrangements (affecting a sphere of 6-8 Å radius around jumping O* ion) and modifications of the chemical bonding character (charge redistribution and bond covalency between O* and Co/Fe). Thus, the migration barrier height cannot be related to a single materials property. This study indicates that the exceptionally low oxygen migration barrier in $Ba_{0.5}Sr_{0.5}Co_{0.8}Fe_{0.2}O_{3-\delta}$ mainly results from the larger (Sr/Ba)*-O* distance compared to ABO_3 perovskites with smaller lattice constant combined with some O*→(Co/Fe) electron transfer (corresponding to increased covalency) which decreases the O*→(Co/Fe) bond length as well as the O* ion size. Further investigations are in progress for the detailed understanding of the oxygen migration process, e.g. variation of the barriers with different A- and B-type cation arrangements, vacancy concentrations and Fe/Co oxidation states etc.

Acknowledgements

The research leading to these results has received funding from the European Union's Seventh Framework Programme FP7/2007-2013 (NASA-OTM) under grant agreement n° 228701 and the US National Science Foundation (NSF) grant n° 0832958. Authors thank NSF for its support through TeraGrid resources provided by Texas Advanced Computing Center (TACC) and the National Center for Supercomputing Applications (NCSA) under grant number TG-DMR100021. MMK is grateful to the Office of the Director of NSF for support under the IRD Program. Any appearance of findings, conclusions, or recommendations, expressed in this material are those of the authors and do not necessarily reflect the views of NSF.

References

1. Y. Teraoka, H.-M. Zhang, S. Furukawa and N. Yamazoe, *Chem. Lett.,* **1985**, 1743 (1985).
2. H. Kruidhof, H. J. M. Bouwmeester, R. H. E. van Doorn and A. J. Burggraaf, *Solid State Ionics,* **63**, 816 (1993).
3. V. V. Kharton, E. N. Naumovich, A. V. Nikolaev, V. V. Astashko and A. A. Vecher, *Russ. J. Electrochem.,* **29**, 1039 (1993).
4. V. V. Kharton, L. Shuangbao, A. V. Kovalevsky, A. P. Viskup, E. N. Naumovich and A. Tonoyan, *Mater. Chem. Phys.,* **53**, 6 (1998).
5. Z. Shao, W. Yang, Y. Cong, H. Dong, J. Tong and G. Xiong, *J. Membr. Sci.,* **172**, 177 (2000).
6. Z. Shao and S. M. Haile, *Nature,* **431**, 170 (2004).
7. L. Wang, R. Merkle and J. Maier, *J. Electrochem. Soc.,* **157**, B1802 (2010).
8. L. Wang, R. Merkle, J. Maier, T. Acatürk and U. Starke, *Appl. Phys. Lett.,* **94**, 071908 (2009).
9. T. Ishigaki, S. Yamauchi, K. Kishio, J. Mizusaki and K. Fueki, *J. Solid State Chem.,***73**, 179 (1988).
10. R. A. De Souza and J. A. Kilner, *Solid State Ionics,* **106**, 175 (1998).
11. E. A. Kotomin, Y. A. Mastrikov, M. M. Kuklja, R. Merkle, A. Roytburd and J. Maier, *Solid State Ionics* (2010) in press, doi: 10.1016/j.ssi.2010.10.011
12. S. Ganopadhyay, A. E. Masunov, T. Inerbaev, J. Mesit, R. K. Guha, A. K. Sleiti and J. S. Kapat, *Solid State Ionics,* **181**, 1067 (2010).
13. H. Zhao, N. Xu, Y. Cheng, W. Wei, N. Chen, W. Ding, X. Lu and F. Li, *J. Phys. Chem. C*, **114**, 17975 (2010).
14. A.G. Kresse and J. Furthmueller, *VASP the Guide*, Univ. Vienna (2003).
15. B. J. P. Perdew, K. Burke and M. Ernzerhof, *Phys. Rev. Lett.,* **77**, 3865 (1996).
16. C. H. J. Monkhorst and J. D. Pack, *Phys. Rev. B,* **13**, 5188 (1976).
17. G. Henkelman, A. Arnaldsson, and H. Jónsson, *Comput. Mater. Sci.,* **36**, 354 (2006).
18. R. D. Shannon, *Acta Crystallogr. Sect. A*, **32**, 751 (1976).
19. J. A. Kilner and R. J. Brook, *Solid State Ionics,* **6**, 237 (1982).
20. S. Svarcová, K. Wiik, J. Tolchard, H. J. M. Bouwmeester, and T. Grande, *Solid State Ionics*, **178**, 1787 (2008).
21. T. Ishihara, H. Matsuda and Y. Takita, *J. Am. Chem. Soc.,* **116**, 3801 (1994).